Food Research International 157 (2022) 111361

Contents lists available at ScienceDirect

Food Research International

journal homepage: www.elsevier.com/locate/foodres

Effect of chlorine sanitizer on metabolic responses of *Escherichia coli* biofilms "big six" during cross-contamination from abiotic surface to sponge cake

Zejia Lin, Tong Chen, Lehao Zhou, Hongshun Yang *

Department of Food Science & Technology, National University of Singapore, Singapore 117542, Singapore
National University of Singapore (Suzhou) Research Institute, 377 Lin Quan Street, Suzhou Industrial Park, Suzhou, Jiangsu 215123, PR China

ARTICLE INFO

Keywords:
Escherichia coli
NMR
Metabolomics
Biofilm
Stainless steel
High-density polyethylene
Flour
Sodium hypochlorite

ABSTRACT

The effect of chlorine on *Escherichia coli* biofilm O157:H7 are well established; however, the effect on biofilm adhesion to food as well as the six emerging *E. coli* serotypes ("big six") have not been fully understood. Chlorine sanitization with 1-min 100 mg/L was applied against seven pathogenic *E. coli* (O111, O121:H19, O45:H2, O26:H11, O103:H11, O145, and O157:H7) biofilms on high-density polyethylene (HDPE) and stainless steel (SS) coupons, respectively. Using sponge cake as a food model, the adhesion behavior was evaluated by comparison of bacteria transfer rate before and after treatment. Besides, the metabolic profiles of biofilms were analyzed by nuclear magnetic resonance (NMR) spectrometer. A significant decrease in transfer rate (79% decline on SS and 33% decline on HDPE) was recorded as well as the distinctive pattern between SS and HDPE coupons was also noticed, with a low population (6–7 log CFU/coupon) attached and low survivals (0–3 log CFU/coupon) upon chlorine on SS, while high population (7–8 log CFU/coupon) attached and high survivals (5–7 log CFU/coupon) on HDPE. Moreover, O121:H19 and O26:H11 demonstrated the highest resistance to chlorine with the least metabolic status and pathways affected. O103:H11, O145, and O111 followed similar metabolic patterns on both surfaces. Distinct metabolic patterns were found in O45:H2 and O157:H7, where the former had more affected metabolic status and pathways on SS but less on HDPE, whereas the latter showed an opposite trend. Overall, a potential contamination source of STEC infection in flour products was demonstrated and metabolic changes induced by chlorine were revealed by NMR-based metabolomics, which provides insights to avoid "big six" biofilms contamination in food.

1. Introduction

Biofilms are complex and highly organized microbial communities that could be grown on abiotic as well as biotic surfaces (Shen et al., 2012). The establishment of biofilms in food-processing environments acts as an effective barrier and recalcitrant to disinfectants as well as antimicrobial agents (von Hertwig, Prestes, & Nascimento, 2022; Wang, Jin et al., 2021). These biofilms contribute to the persistence of bacterial cells on food-contact surfaces such as utensils and equipment, which in turn cause cross-contamination of food (Merino, Procura, Trejo, Bueno, & Golowczyc, 2019; Tan & Karwe, 2021). In our previous research, the propensity of foodborne pathogen to adhere to food-contact materials, as well as food product surfaces has been well demonstrated (Chen et al., 2022; Wu, Zhao, Lai, & Yang, 2021; Zhao et al., 2022). Thus, biofilm generated by pathogenic bacteria on these surfaces is a primary concern of food safety, which may result in an elevated risk of public health and damage to consumer confidence in food safety.

Among biofilm-forming pathogens, Shiga toxin–producing *Escherichia coli* (STEC) is the most common pathogen discovered in flour and flour-associated products according to the US Food and Drug Administration (FDA, 2022). Symptoms of foodborne STEC infections usually include diarrhea, hemolytic uremic syndrome, kidney failure or even death at worst (Wang, Sang et al., 2021). The most notorious STEC in the US is *E. coli* O157:H7, which contributed to 40% of total *E. coli* infections, while other STEC serogroups (namely *E. coli* O45, O26, O145, O111, O121, and O103) were also culprits for serious cases, and they are collectively known as the "big six" (Chen, Zhao, & Wu, 2020). Over the past decade, numerous outbreaks of "big six" associated with wheat

* Corresponding author at: Department of Food Science & Technology, National University of Singapore, Science Drive 2, Singapore 117542, Singapore.
E-mail address: fstynghs@nus.edu.sg (H. Yang).

https://doi.org/10.1016/j.foodres.2022.111361
Received 17 February 2022; Received in revised form 19 April 2022; Accepted 10 May 2022
Available online 13 May 2022

flour have been reported in North America (Centers for Disease Control and Prevention, 2021). However, STEC is commonly found in animal-derived foods, the source of flour contamination remains unknown. Therefore, a potential route of STEC infection in flour products is proposed that flour was cross-contaminated by food-contact surfaces that may get STEC infections from animals, feces, dust, or insects. Study has demonstrated *E. coli* biofilms on surfaces can adhere to food after brief contact, with a transfer rate of 25%-97% (Miranda & Schaffner, 2016).

The sanitization of food-contact surface is usually achieved by chemical disinfectants, such as chlorine, quaternary ammonium compound, and peracetic acid (Sheng, Zhang, Sun, & Wang, 2020; Tan et al., 2022). In addition, a novel application, the combination of electrolyzed water (EW) and ultrasound was evaluated for bacterial biofilm inhibition on stainless steel surfaces in our previous research (Zhao, Li, & Yang, 2021; Zhao, Zhang, & Yang, 2017). However, the most often used disinfectant is chlorine bleach, which is represented by sodium hypochlorite (NaOCl) for its convenience, excellent sterilization, and cost-effectiveness (Byun, Han, Yoon, Park, & Ha, 2021; Li et al., 2020). The US Environmental Protection Agency (2020) allows the use of chlorine sanitizer on food-contact surfaces as well as food processing equipment with a maximum concentration of 200 mg/L available chlorine. Chlorine bleach could generate high oxidation–reduction potential (ORP), and lead to oxidative stress to the bacteria, and meanwhile, its efficacy is determined by the concentration, contact time, and contact surface (Guo et al., 2020). Previous research has evaluated the efficacy of chlorine sanitizer against the *E. coli* biofilm on various food-contact surfaces. Weerarathne et al. (2021) reported a nearly 5-log reduction of *E. coli* O157:H7 on stainless steel (SS) and high-density polyethylene (HDPE), respectively after exposure to 5-min chlorine treatment. However, little research has focused on the effect of chlorine on the adhesion of *E. coli* biofilm as well as bacterial metabolic responses on the food-contact surface, not to mention the strain-specific *E. coli* "big six" biofilms.

As chlorine cannot eradicate the *E. coli* biofilm, it is necessary to evaluate the capability of surviving cells to adhere to food and cause cross-contamination subsequently. Besides, surviving bacteria would undergo a series of metabolic alterations that occur in response to sub-lethal stress and improve their survivability (Han et al., 2018). With the utilization of nuclear magnetic resonance (NMR) spectroscopy, a global picture of physiological process change within the cell under chlorine stress is available, which contributes to a better knowledge of chlorine antibacterial processes as well as the corresponding defense mechanisms adopted by various *E. coli* strains biofilms (Rahman et al., 2019).

Therefore, this research aimed to assess the attachment ability of seven strains of *E. coli* biofilms on SS and HDPE surfaces to food upon chlorine treatment, using the concept of transfer rate and sponge cake as the model of flour product. Furthermore, the metabolomic changes of each biofilm on different surfaces induced by chlorine stress were discovered by NMR spectroscopy, revealing insights into cellular responses to hostile environments. This study will broaden our understanding of strain-specific biofilm response mechanisms and offer guideline to avoid cross-contamination from food-contact surface to food.

2. Materials and methods

2.1. Bacterial strains and culture condition

Seven *E. coli* strains of different serotypes [*E. coli* O145 (ATCC BAA-2192), O103:H11 (ATCC BAA-2215), O45:H2 (ATCC BAA-2193), O111 (ATCC BAA-2440), O121:H19 (ATCC BAA-2219), O26:H11 (ATCC BAA-2196) and O157:H7 (ATCC 35150)] were collected from Department of Food Science & Technology, National University of Singapore (https://www.atcc.org/-/media/resources/brochures/big-six-non-o157.pdf?rev=ef81e3bef584471aa29eb35f07cc433a). Each strain was activated from its glycerol stock solution by transferring into 10 mL of tryptone soya broth (TSB, Sigma-Aldrich, St. Louis, MO, USA) and incubating them overnight at 37 °C, after which were subsequently acclimatized to nalidixic acid (100 μg/mL) (Sigma-Aldrich, St. Louis, MO, USA) by subsequent reinoculation with incremental increases in nalidixic acid concentration. The medium used in this research were also added with 100 μg/mL nalidixic acid. The adopted strain was inoculated into 40 mL of TSB and incubated overnight at 37 °C before use. Each strain of culture was centrifuged for 10 min at 3600 *g* (23 °C). The cell pellet was resuspended twice in 10 mL of peptone water (PW, Oxoid, Basingstoke, UK), centrifuged, and resuspended in PW for the following biofilm inoculation procedure.

2.2. Food-contact surface materials preparation and biofilm inoculation

In this investigation, stainless steel (type 304) and HDPE (smooth finish) surfaces were employed. Before usage, coupons (5 cm × 2 cm) were immersed in a detergent solution overnight before being degreased with ethanol (70%), fully washed by tap water and again by distilled water, dried in air, and autoclaved. The surface roughness as well as the surface charge of the coupons was measured by a 3D optical profiler (Zygo New View 7100) and a Surpass Electrokinetic Analyzer (Anton Paar GmbH, Graz, Austria) at pH 7.0, respectively.

20 mL of sterile low nutrition TSB (LN-TSB, 1:10 dilution of normal TSB solution) were prepared, after which cell suspensions were mixed with at a dilution of 1:100. To facilitate bacterial adhesion on coupons, each coupon was soaked in the suspensions for 4 h at ambient temperature before being drained and gently washed in a circular movement for 10 s with 1 mL PW to remove loosely attached bacteria. The coupon was then incubated again at ambient temperature with 10 mL fresh LN-TSB. After 48 h, the LN-TSB was disposed of, and the coupon was transferred to new LN-TSB solutions for another 24 h at ambient temperature. Following incubation, the coupon was gently washed twice with 1 mL PW to remove loosely adhering cells before drying for 2 h in a biosafety cabinet (Zhao et al., 2022).

2.3. Chlorine sanitization of biofilm on the coupons

Commercial chlorine bleach (5% sodium hypochlorite, Fairprice, Singapore) was purchased and diluted to 100 mg/L before use. Based on our preliminary study (data not shown) and other research (Luu, Chhetri, Janes, King, & Adhikari, 2021; McGlynn, 2004), inoculated coupons were soaked in 100 mL of chlorine solution for 1 min to ensure sufficient *E. coli* with chlorine- induced metabolites survived for the following NMR analysis. In addition, coupons treated with deionized water (DW) were used as the control groups. After that, coupons were transferred into Dey–Engley (Sigma-Aldrich, St. Louis, MO, USA) neutralizing broth for 1 min to neutralize residual chlorine and placed in a biosafety cabinet for drying.

2.4. Transfer between surface and cake

The transfer rate from the food-contact surfaces to cakes was evaluated by placing the inoculated coupon in contact with cake. Sponge cakes were purchased from a local bakery in Singapore on the day of the experiment. The texture profile of sponge cake was analyzed by a texture analyzer (Stable Micro Systems Co. Ltd., Godalming, UK), with a testing speed of 1 mm/s, and a compression distance of 10 mm. The measurement of textural parameters consists of cohesiveness, springiness, hardness, gumminess, and resilience. In addition, the specific volume of the cake was determined by a Volscan profiler (Stable Micro System Ltd, Surrey, UK). Each coupon was sandwiched between cakes (20 g) and remained in contact for 5 min to ensure sufficient time for cells to adhere to surfaces. The coupon was then put into a sterile tube (50 mL) with 20 mL PW plus 20 glass beads (5 mm), and the adhered cells were detached from the coupon by vertexing at full speed for 1 min. Cakes were placed into a stomacher bag with 180 mL of PW and homogenized for 1 min

(Masticator Stomacher, IUL Instruments, Germany). Samples from coupon and cake were serially diluted in 0.1% PW, respectively before being plated (100 μL) onto tryptic soy agar ((TSA, Sigma-Aldrich, St. Louis, MO, USA)) for *E. coli* bacterial counting. Plates were then incubated at 37 °C for 24 h, after which the population of colonies was enumerated, and the results were expressed as colony forming units (CFU) per cake or coupon. The total CFU and the transfer rate (%) was calculated as follows:

$$\text{Total CFU} = \text{CFU/cake} + \text{CFU/coupon}.$$
$$\text{Transfer rate (\%)} = (\text{CFU/cake})/(\text{total CFU}) \times 100.$$

2.5. Extraction of E. coli biofilm metabolites

The metabolomics study was performed on *E. coli* biofilm on coupons with and without chlorine treatment, using a method described by Wang and Wu (2022) with certain changes. For each strain, 10 pieces of coupons were prepared as described in 2.3 and the glass beads vortex method in 2.4 was applied to detach bacteria from coupons, after which the bacteria suspensions were centrifuged for 10 min at 16,000 *g* (4 °C), and the cell pellets were suspended in 20 mL of TSB and incubated for 6 h at 37 °C to acquire sufficient amount of metabolites. The cell suspensions were once again centrifuged for 10 min at 16,000 *g* (4 °C), resuspended with 5 mL of PW twice, and then mixed well in 1 mL of ice-cold methanol-d_4. To disrupt the membrane structure, liquid nitrogen was used to freeze the samples, which were then thawed three times on ice. The extraction was then carried out overnight at −20 °C, followed by centrifugation for 20 min at 12,000 *g* (4 °C). As an internal reference, 10 mmol/L trimethylsilyl propanoic acid (TSP, dissolved in methanol-d_4) was mixed with the acquired extract with a dilution of 1:10. The resulting supernatant (630 μL) was subject to an NMR test.

2.6. NMR spectroscopic analysis

The NMR experiments were run by an NMR spectrometer (Bruker DRX-500, Rheinstetten, Germany) at 298 K with a triple inverse gradient probe. The ^{1}H spectrum of each sample was obtained for metabolic analysis with a first increment of the NOESY standard pulse sequence. The data were acquired in a spectral width of 10 ppm. Before the Fourier transformation, an exponential window function with a widening factor of 1 Hz was used to handle all free induction decays. In addition, the 2D ^{1}H–^{13}C heteronuclear single quantum coherence spectroscopy (HSQC) was performed on a single *E. coli* strain at 298 K to assign resonance and identify metabolites. The F1 and F2 channels were used to evaluate ^{13}C spectra with a width of 175 ppm and ^{1}H spectra with a width of 10 ppm, respectively (He, Zhao, Chen, Zhao, & Yang, 2021).

2.7. Spectral analysis

The resulting NMR data were adjusted for phase distortions and baseline distortions by software TopSpin 4.1.3 (Bruker). The chemical shifts of metabolites were verified using 1D ^{1}H and 2D ^{1}H–^{13}C NMR database from the *E. coli* Metabolome Database (https://www.ecmdb.ca/), and the Human Metabolome Database (https://www.hmdb.ca/). Additionally, Mnova (Mestreab, Research SL, Santiago de Compostela, Spain) was applied to cut the water region (4.50–5.10 ppm), normalize peaks between 0.5 and 10.0 ppm to sum intensities, and bin the spectra into baskets with 0.02 ppm integral width (Mahmud, Kousik, Hassell, Chowdhury, & Boroujerdi, 2015).

Based on the binned data, SIMCA software (version 14.0, Umetrics, Sweden) was utilized to conduct principal component analysis (PCA) to separate each data set, and orthogonal projection to latent structures-discriminant analysis (OPLS-DA) to identify the dissimilarities between control and treatment groups (Vong, Hua, & Liu, 2018). The data of OPLS-DA models were subsequently analyzed using the variable importance in projection (VIP), the fold change (FC), and the corresponding *P* values in each pairwise comparison to screen out significantly altered metabolites that were sensitive to chlorine stress. Finally, screened metabolites were imported into MetaboAnalyst 5.0 (https://www.metaboanalyst.ca/) for enrichment pathway analysis, using the Kyoto Encyclopedia of Genes and Genomes (KEGG) database (https://www.genome.jp/kegg/pathway.html) as a reference (Mahmud et al., 2015).

2.8. Statistical analysis

All experiments were conducted independently in triplicate. One-way analysis of variance (ANOVA) was conducted to analyze the statistical data, using Duncan's multiple range test in SPSS software (version 21; IBM Co., Armonk, NY, USA) to compare the sanitizing efficacy of chlorine against each strain on various surfaces. Differences with $P < 0.05$ were defined as statistically significant.

3. Results and discussion

3.1. Effects of chlorine on transfer rate from various types of coupons to cakes

The transfer experiment results of seven *E. coli* strains biofilms from surfaces to cakes upon various treatment are shown in Fig. 1 as well as the textural profile of sponge cake in Table S1. Fig.1A1-A2 show the change of bacterial population on SS and HDPE coupons before and after chlorine treatment, while Fig.1B1-B2 describe the change of attached cells on cake before and after contacting with SS and HDPE, respectively. After chlorine sanitization, a huge decline in transfer rate from various types of coupons to cakes was observed. More specifically, the transfer rates of seven *E. coli* strains biofilms from SS to cakes were found to drop to 0% ($P < 0.05$) after chlorine (Fig. 1C1). Meanwhile, significant reductions of transfer rates ($P < 0.05$) from HDPE to cakes were only recorded in O157, and O45 (Fig. 1C2).

Overall, our finding suggested that chlorine-induced damage can compromise the biofilm surface adhesions. On the one hand, the adhesion capability of biofilm is mediated by extracellular polymeric substances (EPS), which are the major component of biofilm (Kim, Kim, & Kang, 2020). A positive correlation between biofilm adhesion capability and EPS content was reported (Ying, Yang, Bick, Oron, & Herzberg, 2010). Upon exposure to NaOCl, EPS would interact with it first as a sacrificial barrier. Studies have demonstrated that NaOCl attacked functional groups in EPS, which changed the EPS physicochemical properties and made them easier to detach from the surfaces (Xue, Sendamangalam, Gruden, & Seo, 2012).

On the other hand, proteinous cell appendages (e.g., pili, flagella) are important for the initial adhesion between cells and contact subjects. Flagella are engaged in bacterial adhesion in two ways: indirectly through motility toward targets, and directly through adherence to them (Haiko & Westerlund-Wikström, 2013). Chlorine could not only damage the flagella by causing protein denaturation but also depress the expression of flagella-associated genes (*flgC*, *ompF*, and *traG*), resulting in fewer flagella appearing on cells (Liu et al., 2021). Furthermore, it has been suggested that *E. coli* might adopt an energy conservation strategy for survival in adverse environmental conditions (Zhao et al., 2022), which might lead to a decline of flagella motility due to insufficient energy.

The total CFU of *E. coli* from HDPE (7.18–8.14 log CFU/coupon) was higher than that from SS (5.96–7.46 log CFU/coupon). Although the mechanism of cell adhesion to surfaces is not well understood, it has been reported that surface properties such as hydrophobicity, surface roughness as well as surface charge can mutually affect cell adhesion (Adhikari, Syamaladevi, Killinger, & Sablani, 2015; Bakterij, 2014; Tan, Zhou, Luo, & Karwe, 2021). However, in our study the surface roughness as well as the surface charge of the SS (0.17 μm and −38.71 mV, respectively) and HDPE (0.11 μm and −34.47 mV, respectively) coupon

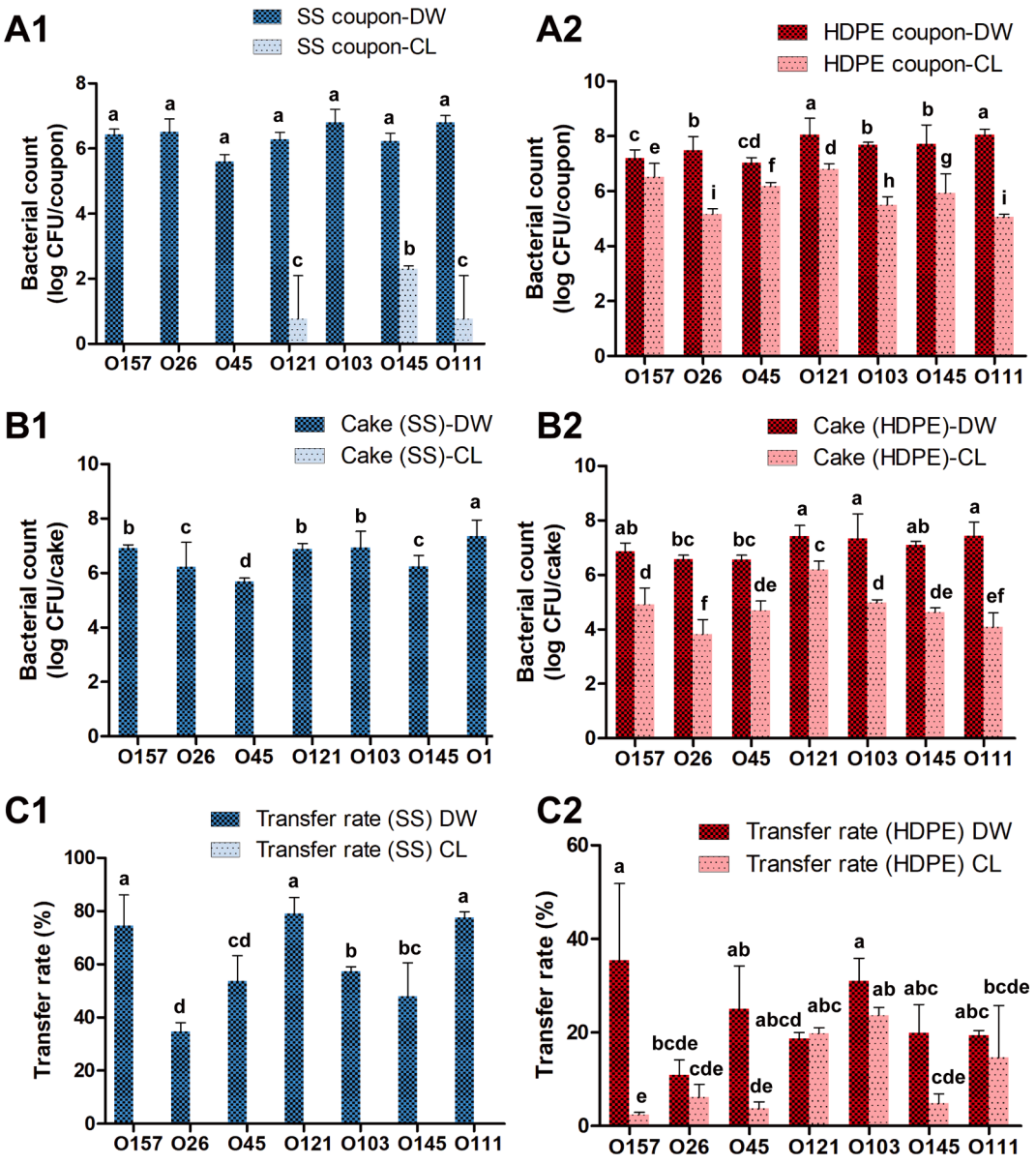

Fig. 1. The transfer experiment of seven *E. coli* strains biofilms from coupons to cake upon deionized water (DW) treatment and chlorine treatment (CL). Means ± standard deviations (n = 3) are used to present the data. The means with different letters vary considerably ($P < 0.05$). Note: A1-A2: Bacterial count of stainless steel (SS) and high-density polyethylene (HDPE) coupon, respectively after contact with cake; B1-B2: Bacterial count of cake after contact with SS and HDPE, respectively; C1-C2: Transfer rate of *E. coli* biofilm from SS and HDPE coupon to cake, respectively.

is approximately the same, which leaves the surface hydrophobicity the main factor in our study. A hydrophobic surface could promote bacterial cell adhesion by pushing the water layer away due to the decreased interaction between the surface and water molecules (Araújo, Bernardes, Andrade, Fernandes, & Sá, 2009). Research have been confirmed that the hydrophobicity of SS surface is lower than that of HDPE surface (Dhowlaghar, Bansal, Schilling, & Nannapaneni, 2018; Kim, Moon, Kim, & Ryu, 2019). In addition, Di Ciccio et al. (2015) found the biofilm formation occurred to a greater extent on the hydrophobic surface than on the hydrophilic surface. Bang et al. (2014) also reported that a higher hydrophobicity of surface resulted in more *E. coli* O157:H7 attachment.

The variance of *E. coli* chlorine susceptibility between SS and HDPE surfaces was also observed. A range of 3.79–7.46-log reduction of total CFU after treatment was recorded on SS while 0.87–3.02-log reduction on HDPE. In general, *E. coli* biofilms displayed higher chlorine resistance on HDPE than that on SS. Although the mechanism of bacterial resistance on different surfaces is not completely understood, the surface hydrophobicity seems to be a decisive factor in our study. A potential explanation was given by Pagedar, Singh, and Batish (2010) that an enhanced adhesion of pathogen to hydrophobic materials contributed to a reduced sanitizing efficiency. In addition, Park and Kang (2017) reported that a lower reduction of *E. coli* O157:H7 upon sanitizer was obtained on a more hydrophobic surface. Other researchers also found similar results (Bang et al., 2014; Kim, Ryu, Park, & Ryu, 2017; Kim et al., 2019).

3.2. Metabolites identification and multivariate analysis

The ^{1}H NMR spectra of seven *E. coli* strains biofilms on food-contact surfaces with and without chlorine treatment is shown in Fig. S1. According to our previous research (Chen et al., 2020; Wang & Wu, 2022), 2D NMR analysis (^{1}H–^{13}C HSQC), and the metabolites database, the ^{1}H, and ^{13}C resonances were ascribed to certain metabolites. (Table S2). 40

metabolites were identified in the biofilms of seven *E. coli* strains, including organic acids, amino acids, sugars, nucleotides, and other metabolites.

PCA was utilized to analyze disparities between metabolomes and identify group variances in order to well understand the variety among seven *E. coli* strains biofilms under different conditions. Fig. 2 depicts the model quality and grouping information as determined by the model quality parameters and the 3D score plots, respectively. For *E. coli* biofilms on SS, the first three principal components (PCs) of biofilms treated with DW and the first five PCs of biofilms treated with chlorine explained 87.3% and 96.6% of the total data, respectively. In addition, for *E. coli* biofilms on HDPE, the first five PCs of biofilms treated with

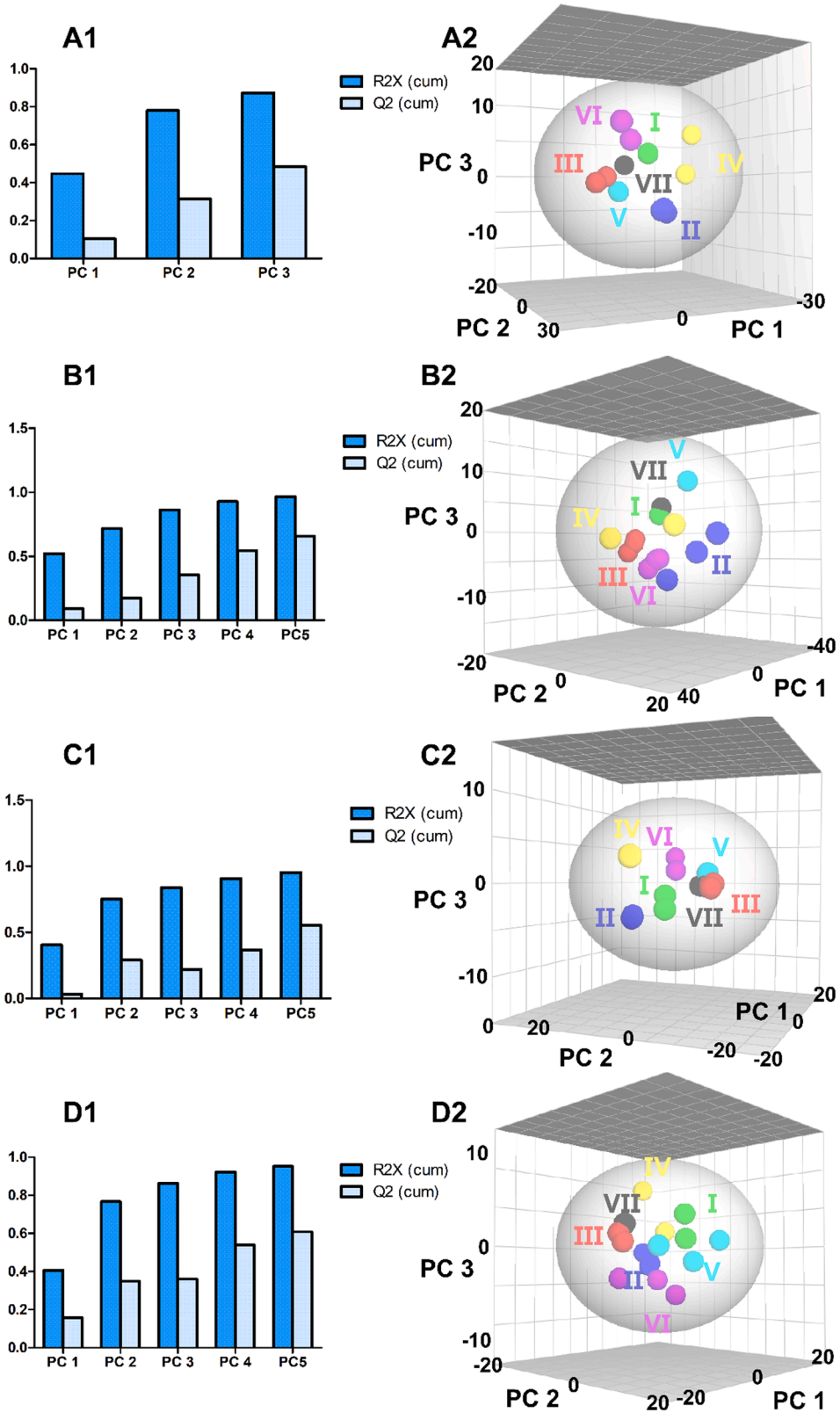

Fig. 2. Principal component analysis (PCA) of ^{1}H NMR spectra of seven *E. coli* strains biofilms upon various treatments. The variances are explained by principal components in PCA (A1-D1); and the 3D score plot of PCA (A2-D2). Note: A: stainless steel (SS) surfaces treated with deionized water (DW); B: SS surfaces treated with chlorine; C: high-density polyethylene (HDPE) surfaces treated with deionized water (DW); D: HDPE surface treated with chlorine; I: O157:H7; II: O145; III: O121:H19; IV: O111; V: O103:H11; VI: O45:H2; VII: O26:H11.

DW, and those with chlorine explained 95.3% and 95.1%, respectively (Fig. 2A1-D1). The Q^2 values for these four groups ranged from 0.48 to 0.66. Although the Q^2 value of biofilms on SS with DW treatment (0.48) did not exceed 0.5, the predictive model was still acceptable for $Q^2 > 0.4$ (Munir et al., 2020). Overall, the R^2X and Q^2 values of the remaining groups indicated that the models were of high quality, with high interpretability and predictability (Chen et al., 2020). Within each treatment group, seven strains of *E. coli* biofilms generally exhibited clear separations in the 3D score plots, except O157 and O26 on SS treated with chlorine, and O121, O103, and O26 on HDPE with DW, respectively, which suggested that under certain conditions some of the strains might show similar metabolic responses (Fig. 2A2–D2).

OPLS-DA generated from the identified metabolites of control and treatment groups on both contact surfaces was performed to further investigate the metabolic responses of each strain associated with different treatments. The results are presented in the form of cross-validated score plots and corresponding coefficient plots (Fig. 3, Fig. 4, Fig. S2 and Fig. S3). The R^2X and Q^2 values (close to 1) illustrated that these OPLS-DA models had good fitness and predictability (Table S3). The score plots of these models established definite separations between groups, implying that the metabolic responses of each *E. coli* strain biofilm with or without chlorine sanitization can be distinguished. The relevant coefficient plots were also used to screen the metabolites that contributed potentially to the pairwise differentiation with columns pointing downward and upward indicate lower and greater relative contents, respectively between the control group and the chlorine treatment group.

The pairwise comparison of metabolites between SS and HDPE surfaces was also conducted, using OPLS-DA. Not surprisingly, good models with high fitness and predictability, and clear separations between SS

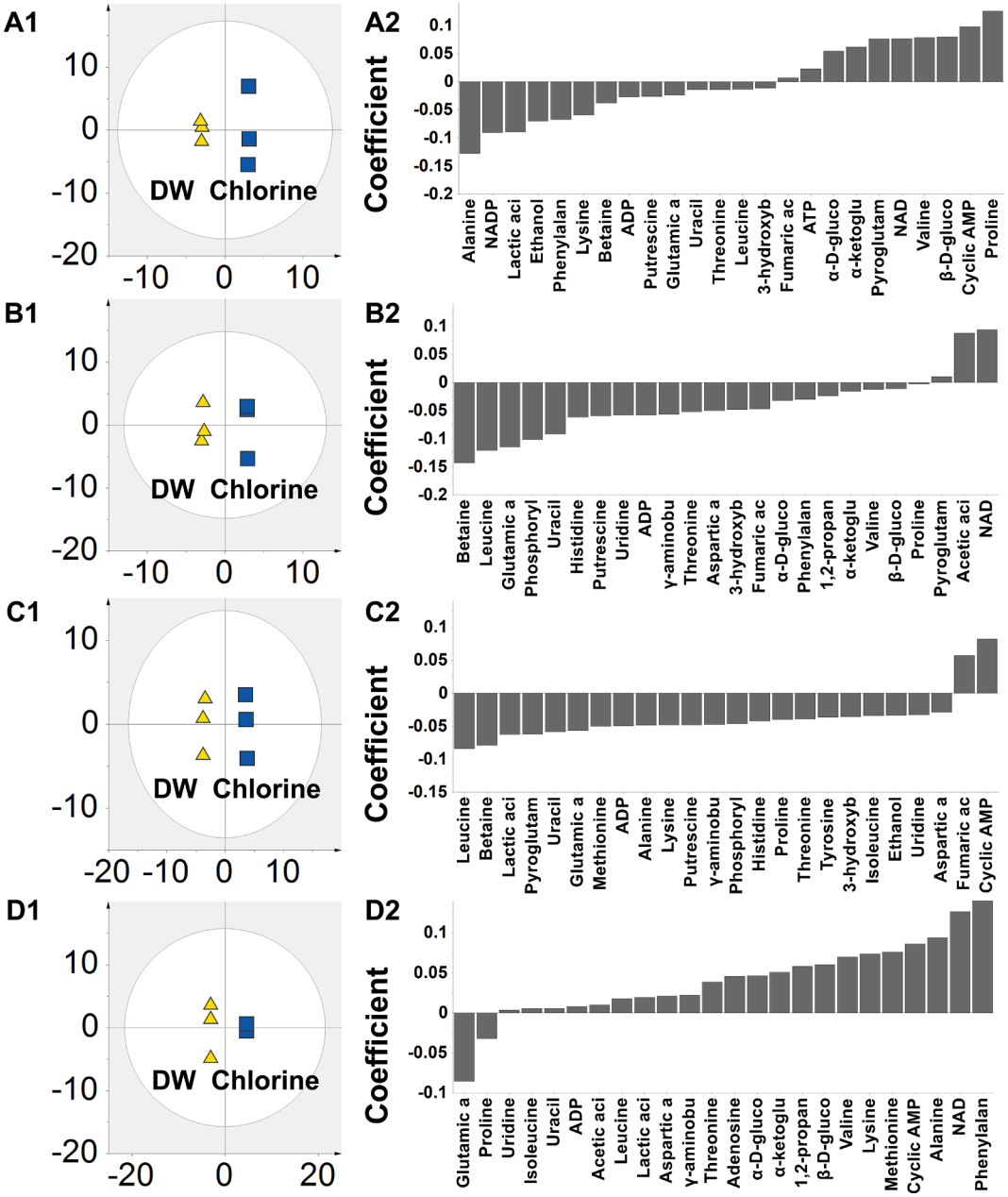

Fig. 3. Orthogonal projection to latent structures-discriminant analysis (OPLS-DA) of each *E. coli* biofilm on stainless steel (SS) surfaces between control and treatment groups. Note: A1-A2: Score plot and coefficient plot of O157:H7; B1-B2: Score plot and coefficient plot of O121:H19; C1-C2: Score plot and coefficient plot of O103; D1-D2: Score plot and coefficient plot of O45:H2.

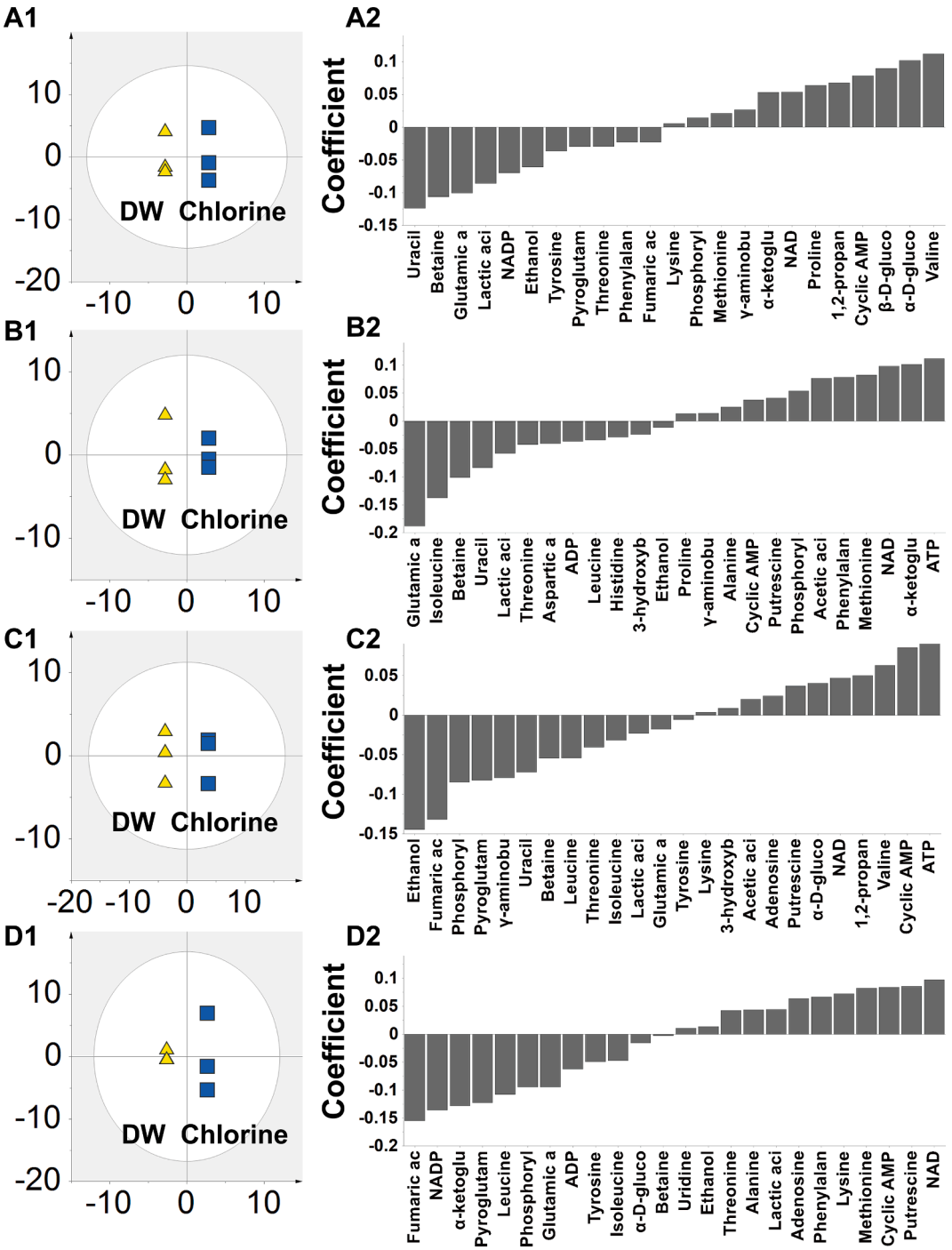

Fig. 4. Orthogonal projection to latent structures-discriminant analysis (OPLS-DA) of each *E. coli* biofilm on high-density polyethylene (HDPE) surfaces between control and treatment groups. Note: A1-A2: Score plot and coefficient plot of O157:H7; B1-B2: Score plot and coefficient plot of O121:H19; C1-C2: Score plot and coefficient plot of O103; D1-D2: Score plot and coefficient plot of O45:H2.

and HDPE groups were achieved in all strains except for O157 with DW, O121 with chlorine, and O26 with both treatments (Fig. S4, Fig. S5, and Table S4). These results once again evidenced the variance of *E. coli* biofilms between SS and HDPE surfaces, which offered the metabolic basis for their difference of the initial population and chlorine resistance on SS and HDPE discussed in 3.1.

3.3. Alternative metabolites in E. coli biofilms under chlorine stress on various food-contact surfaces

Metabolites shown in the coefficient plots with a VIP > 1, a fold change (FC) > 1.20 or < 0.83, and a P value < 0.05 (He et al., 2021) were further screened out and summarized in Table 1, which indicated the significantly affected metabolites in each *E. coli* strain biofilm after chlorine treatment. Overall, on SS surfaces, O45 exhibited the most metabolites (14) significantly altered, followed by O145, O111, and O103 (13, 12, and 11, respectively). O121, O26 and O157 were found be to the least affected with 6 metabolites changed. On HDPE surfaces, the affected metabolites in O145, O111, and O103 were similar to that on SS, whereas O45 exhibited only 7 significantly affected metabolites, reaching the same level of O121 and O26 (5 and 7, respectively).

A schematic model illustrating the variance of seven *E. coli* strains

Table 1
Metabolites significantly altered in each *E. coli* strain biofilm after 1-min chlorine (100 mg/L NaClO) treatment.

Metabolite category	Contact surface	Metabolite	Strains showing significant increase (VIP > 1; FC > 1.2; $P < 0.05$)	Strains showing significant decrease (VIP > 1; FC < 0.83; $P < 0.05$)
Amino acids	SS	Ala	O103	O111; O45
		Asp	O145	
		Glu	O103; O111; O145; O157	
		His	O145	
		Leu	O103; O111; O145	
		Lys	O45	
		Met	O103	O45
		Phe		O45
		Pro		O157
		Thr	O103; O145	O45
		Val		O45
	HDPE	Glu	O103; O111; O145; O157; O45	
		His	O145	
		Ile	O103; O111; O145; O26	
		Leu	O103; O111; O145	
		Lys	O45	
		Met		O45; O26
		Pro		O157
		Thr	O103; O145	
		Val		O103
Organic acids	SS	Acetic acid		O111; O121
		Fumaric acid	O111; O26;	
		Lactic acid	O111; O26; O103; O157	
		α-ketoglutaric acid		O111; O45
		γ-aminobutyric acid	O103	O45
	HDPE	3-hydroxybutyric acid	O145	
		Acetic acid		O111; O121
		Fumaric acid	O111; O26; O103	
		Lactic acid	O111; O145; O103; O157	
		Pyroglutamic acid	O103; O45	
		α-ketoglutaric acid	O111; O145	O121
		γ-aminobutyric acid	O103	
Alcohols	SS	Ethanol	O145	
		1,2-propanediol		O45
	HDPE	Ethanol	O103; O157	O45
		1,2-propanediol		O157
Sugar	SS	α-D-glucose		O45
		β-D-glucose	O145; O26	O111; O45
	HDPE	α-D-glucose	O145	O103; O111; O157
		β-D-glucose	O145	O157
Nucleotide related compounds	SS	Adenosine		O45
		ATP		O111
		Cyclic AMP		O111; O145; O157; O26; O45
		NAD		O111; O121; O145; O157; O45
		Uracil	O103; O121; O145	
		Uridine	O121	
	HDPE	Adenosine		O45
		ATP		O121
		ADP	O145	
		Cyclic AMP		O103; O111; O145; O26
		NADP	O157	
		NAD		O111; O121; O145; O103; O45
		Uracil	O103; O145; O157; O26	
Others	SS	Betaine	O111: O121; O145; O157; O26; O103	
		Phosphorylcholine	O103; O121; O145; O26	
		Putrescine	O103; O145	
	HDPE	Betaine	O111: O121; O145; O157; O26	
		Phosphorylcholine	O103	
		Putrescine	O145; O26	O121

Note: SS: stainless steel surface; HDPE: high-density polyethylene surface.

metabolic pattern between SS and HDPE surfaces during chlorine treatment is proposed in Fig. 5 with detailed information which will be discussed below.

A variation pattern of metabolic change was seen in *E. coli* O45 with a high quantity of affected metabolites on SS, but few affected on HDPE. Specifically, 6 markedly altered amino acids were observed to experience a decline on SS, which might suggest that amino acid catabolism was preferred over anabolism in O45 since the amino acid anabolism is particularly susceptible to hostile influences such as oxidative environment (Wang & Wu, 2022). Furthermore, after chlorine treatment, O45 had considerably decreased levels of cyclic AMP, NAD, α-ketoglutaric acid as well as γ-aminobutyric acid (GABA). These metabolites are associated with the TCA cycle and their depletion implied an inadequate energy supply in cell. Meanwhile, sugars (e.g., α-D-glucose, β-D-glucose) decreased significantly, which implied an enhanced glycolysis strategy was adopted to utilize glucose directly for energy supply (Zhang et al., 2020). In contrast, on HDPE surfaces only two amino acids, as well as NAD were significantly decreased, which indicated a less intensive effect of chlorine on HDPE compared with SS.

Generally, *E. coli* O145, O103, and O111 followed a similar metabolic pattern on both surfaces when facing chlorine treatment with variances in the replenishment of energy. Specifically, amino acids were recorded to increase after chlorine treatment on SS surfaces. However, the depletion of TCA associated metabolites was still recorded in O145 and O111 but not in O103, which suggested O103 might not suffer an energy shortage. Additionally, the level of sugars was observed to decline in O111 but increase in O145, as the former might adopted the glycolysis enhancement while the latter focused on the TCA cycle in an energy-efficient way (Wang & Wu, 2022). A heightened level of lactic acid was recorded in O111 and O103, and the accumulation of organic acid or ethanol might suggest a mixed acid fermentation was activated for energy replenishment (Zhao et al., 2022). Moreover, other metabolites (e.g., phosphorylcholine, putrescine, betaine) associated with membrane recovery, antioxidation, and osmo-protection (Geiger, López-Lara, & Sohlenkamp, 2013; Tkachenko, Nesterova, & Pshenichnov, 2001; Zhao, Zhao, Phey, & Yang, 2019), were found to be significantly raised in these three strains on SS, indicating activation of anti-chlorine mechanism. Similarly, on HDPE these three strains demonstrated an upward trend in the level of amino acids, phosphorylcholine, putrescine, and betaine upon chlorine. The level of TCA cycle-associated metabolites was only found to decrease in O145 while remaining steady in others. The depletion of sugars was observed in both O103 and O111 and the accumulation of lactic acid was found in all strains.

E. coli biofilm O157 exhibited a distinct pattern of metabolite change, opposing more metabolites impacted on SS than HDPE. On SS surfaces, TCA cycle-associated metabolites were observed to deplete after chlorine treatment, while betaine and lactic acid were recorded to increase. On HDPE, a similar change was recorded with an additional observation of sugar depletion and ethanol increase, indicating that strain might adopt glycolysis enhancement and mixed acid fermentation simultaneously.

The metabolite variation pattern in *E. coli* biofilm O121 and O26 was also unique. Unlike the majority of other strains, the content of amino acids and sugars remained unaffected after chlorine sanitization on both contact surfaces. On SS surfaces, TCA cycle-associated metabolites were observed to decline in both strains, while the increases of betaine and phosphorylcholine were observed. Similarly, on HDPE surfaces, the depletion of TCA cycle-associated metabolites was recorded. For metabolites related to the anti-chlorine mechanism, only betaine was observed to increase in both strains upon treatment, while putrescine experienced a significant increase in O26 but a decline in O121, which might suggest the oxidative stress of chlorine was less intensive to *E. coli* O121 biofilm on HDPE. Overall, the minimal degree of metabolic alterations indicated O121 and O26 poor sensitivity to chlorine in comparison to the others.

3.4. The change of E. coli biofilms metabolic pathways upon chlorine stress on various food-contact surfaces

Pathway analysis was used to investigate the differences in each strain's metabolic response when subjected to chlorine stress. MetaboAnalyst 5.0 was applied to predict all impacted pathways according to the significant discriminative metabolites filtered out in 3.3, and those with $P < 0.05$ were recognized as crucial pathways alterations, as summarized in Table S5. The pathways alterations of *E. coli* O45, O103, O157, and O121 on SS and HDPE are shown in Fig. 6 and Fig. 7, respectively as representative strains, while the remaining are shown in Fig. S6.

According to the KEGG database, an assumptive schematic map demonstrating the metabolic alterations of all seven *E. coli* strains

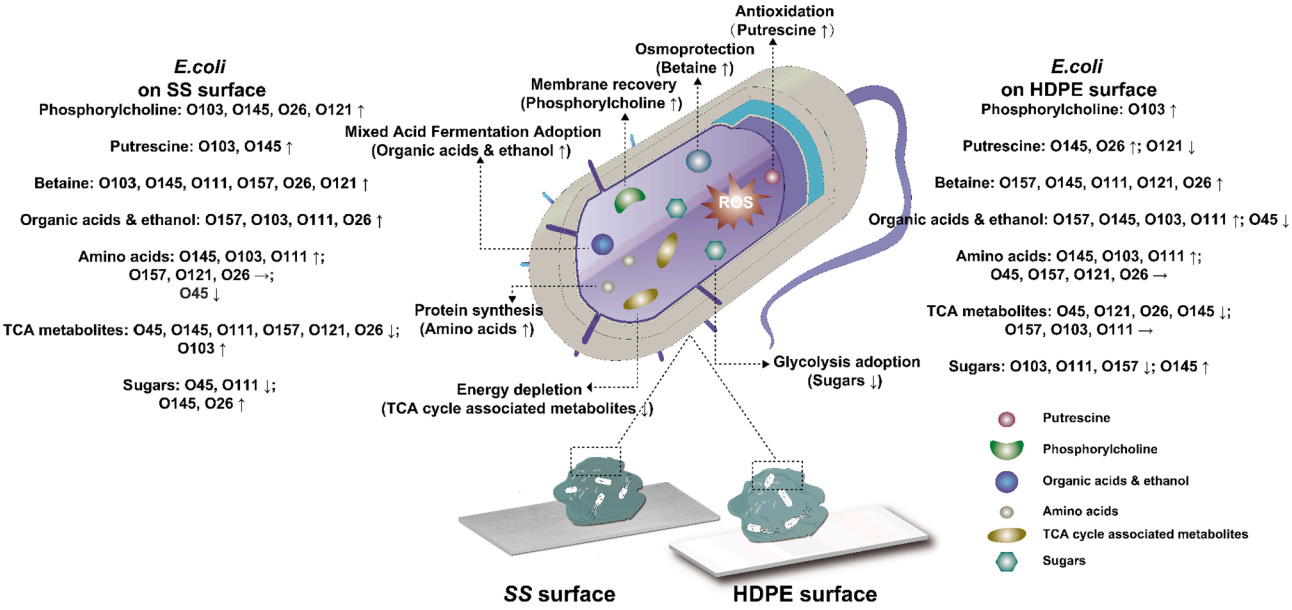

Fig. 5. Proposed schematic of metabolites variation pattern of each strain between high-density polyethylene (HDPE) and stainless steel (SS) surfaces during chlorine treatment. Note: The upward and downward arrows next to measured metabolites indicate greater and lower concentrations, respectively. upon chlorine treatment.

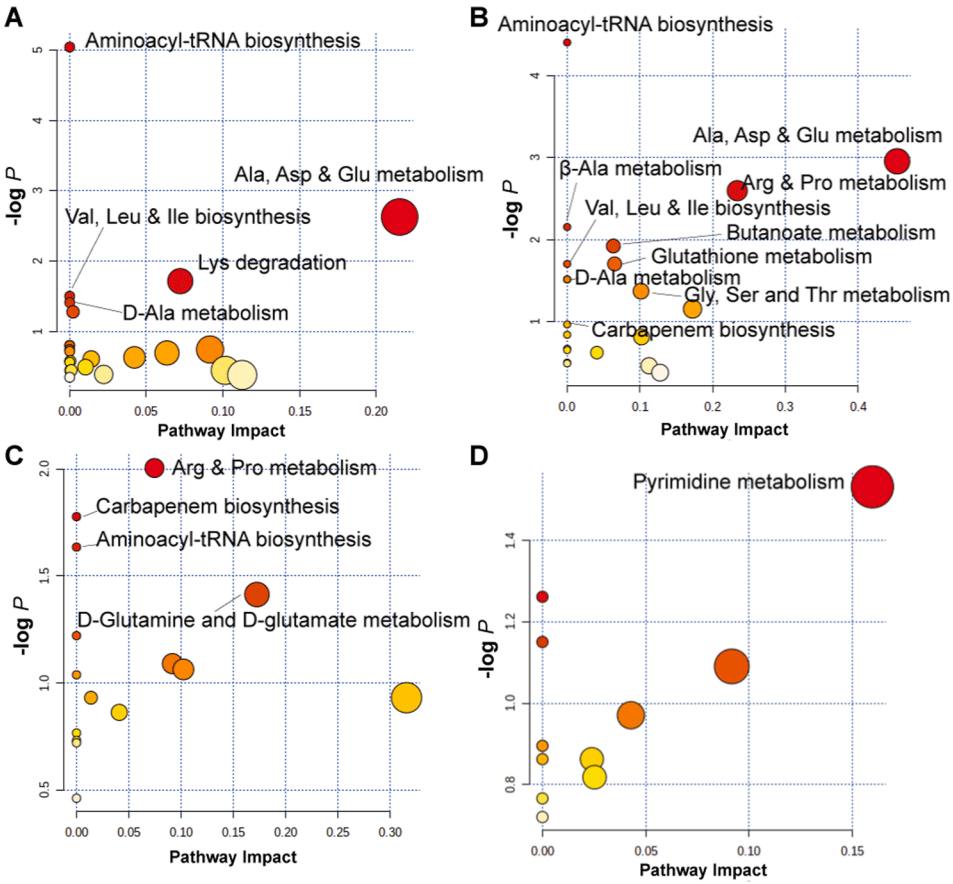

Fig. 6. Metabolic pathways altered by chlorine stress in *E. coli* strain biofilms on stainless steel (SS) surfaces. Note: A: O45:H2; B: O103:H11; C: O157:H7; D: O121:H19.

biofilms upon chlorine exposure is described in Fig. 8. Upwards or downwards arrows suggest a greater or lower level in the chlorine-treated groups compared to the control groups, while no arrow means unchanged level. Overall, the most affected pathway on both surfaces was amino acid metabolism. Elevated levels of the majority of amino acids suggested the *E. coli* biofilm had activated certain resistance mechanisms against chlorine stress. For instance, the antioxidant systems in *E. coli* are regulated by *soxRS* and *oxyR* genes, which could be activated upon HOCL and synthesize SoxS, SoxR, and OxyR protein (Lushchak, 2011). Therefore, the increase of Leu and Ile in O103, O111, and O145 on both surfaces after chlorine treatment might suggest a special protein synthesis mechanism among certain strains in response to oxidative stress (Zhao et al., 2022). Additionally, glutamate was observed to increase in most strains on both surfaces, acting as osmotic regulators as well as various stress-related metabolites' precursors, such as putrescine and GABA (Wang & Wu, 2022; Zhao, Chen, Wu, He, & Yang, 2020). Previous research also found that chlorine-induced stress could accelerate the growth of *E. coli*, which could partly explain the increase of most amino acids (Kwak, Jo, & Yoon, 2014).

Contrary to the upward trend of amino acids in other strains, most amino acids in O45 were found to decline as mentioned in 3.3, which appeared to be more sensitive to chlorine treatment. Specifically, Ala, Val, Met, Phe, and Thr were found to decline on SS and Met on HDPE. Ala, Val, Thr, and Pro are osmoprotectants, maintaining the stability of cytoplasm osmolality when exposed to osmotic stress (Winaya & Maftuchah, 2020), while Met is sulfurous amino acid, which was reported to be more susceptible to oxidative stress (Yang et al., 2019). Thus, the depletion of these amino acids in O45 suggested that when faced with chlorine, the ability to maintain the cytoplasmic osmolality might be compromised on SS. Besides the decline of Pro was observed in O157 on both surfaces, which implied that O157 may also experience a minor impairment in maintaining osmotic homeostasis in the presence of chlorine. The amino acid metabolism of O121 and O26 were barely altered, with none and two amino acids markedly affected, respectively on both surfaces, which once again evidenced that these two strains exhibit high resistance toward chlorine.

A marked decline of TCA associated metabolites in most strains implied the disturbance of the TCA cycle and energy shortage, though the enhanced amino acid metabolism could supply more carbon skeletons into the TCA cycle (He et al., 2021). Previous research found that NaClO-induced stress led to an impairment in cellular energy metabolism by triggering the downregulation of NADH dehydrogenase genes in Complex I and fumarate reductase genes in Complex II. The former catalyzes the conversion of NADH to NAD and the latter catalyzes the conversion of fumarate to succinate during the anaerobic pathway (Small, Chang, Toghrol, & Bentley, 2007). Thus, the associated gene repression led to the depletion of NAD in most strains except for O26, and the accumulation of fumaric acid in O111, O26, and O103.

Alternatively, some strains might adopt to non-TCA pathway for energy replenishment. A significant decline of glucose was found in *E. coli* O111, O45, O157, and O103, implying that they might obtain energy directly from glucose via glycolysis. It has been reported that under stress conditions *E. coli* might take glycolysis as a primary energy source (Wang & Wu, 2022; Zhang et al., 2020). In addition, the glycolytic flux of *E. coli* is determined by ATP/ADP ratio, and a lower ratio would stimulate an enhancement of glycolysis (Koebmann, Westerhoff, Snoep, Nilsson, & Jensen, 2002). Simultaneously another strategy could be adopted for energy compensation. The increased level of lactic acid or ethanol in *E. coli* O111, O103, O145, O26, and O157, suggested these strains might switch from aerobic oxidation to mixed acid fermentation

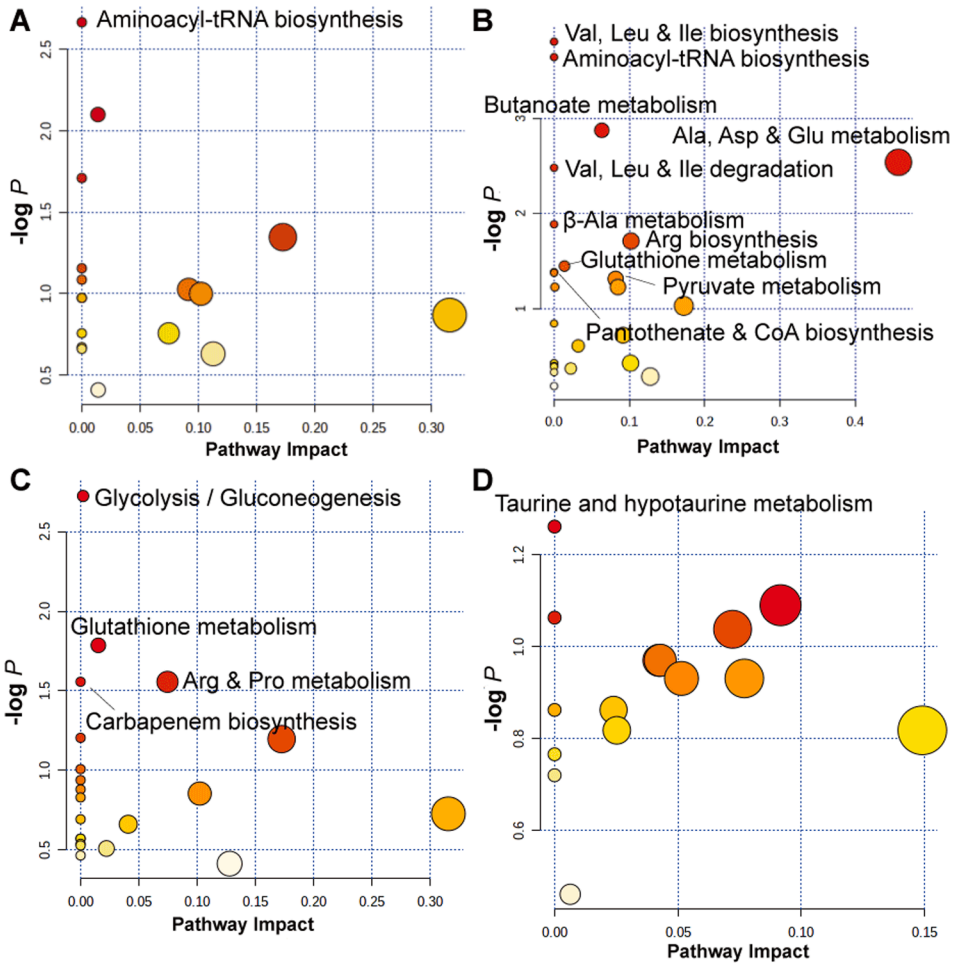

Fig. 7. Metabolic pathways altered by chlorine stress in *E. coli* strain biofilms on high-density polyethylene (HDPE) surfaces. Note: A: O45:H2; B: O103:H11; C: O157:H7; D: O121:H19.

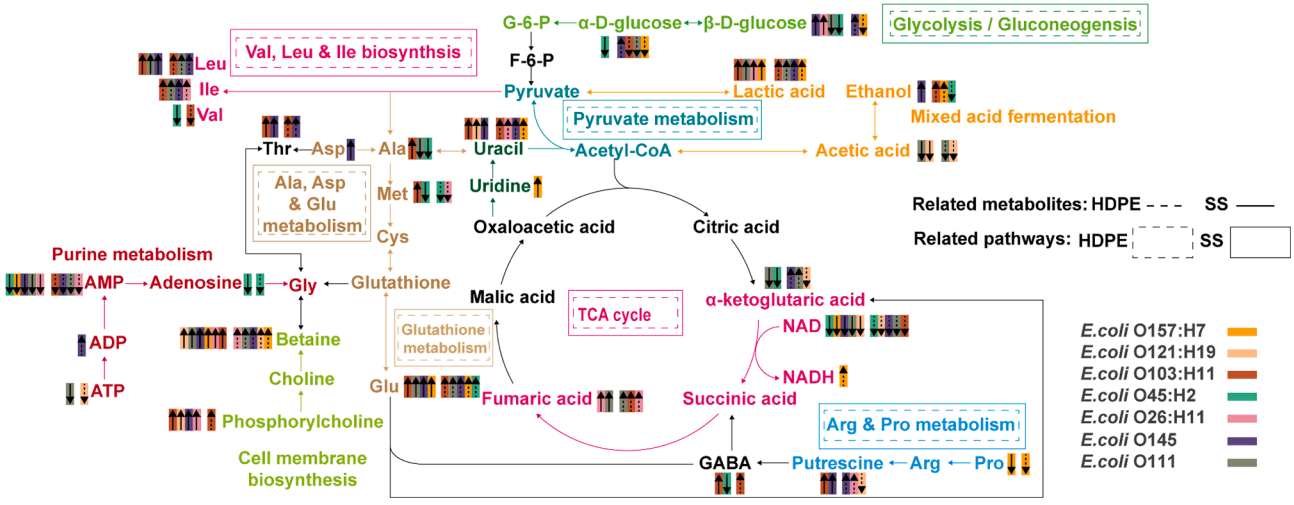

Fig. 8. Proposed schematic of chlorine-induced metabolic changes in seven *E. coli* strains biofilms on high-density polyethylene (HDPE) surfaces and stainless steel (SS). Note: The main pathways affected on SS and HDPE surfaces are framed in solid and dashed boxes, respectively. Solid arrows: metabolite changes on SS; Dashed arrows: metabolite changes on HDPE.

to acquire energy.

The activation of anti-chlorine metabolism in *E. coli* biofilm was also recorded. The boost of putrescine was observed in O145, O103, and O26. Previous research has confirmed that upon NaClO-induced stress, putrescine could stimulate the expression of *oxyR* genes in *E. coli* (Tkachenko et al., 2001). OxyR proteins play an significant part in the antioxidant system, which regulates the expression of many oxidation-inducible activities, including glutathione reductase (*gorA*), alkyl

hydroperoxide reductase (*ahpCF*), and hydroperoxidase I (catalase, *catG*) (Liu et al., 2020). Thus, the elevated level of putrescine might indirectly help the cell to ease the reactive oxygen species and improve the reduced form of redox couples (Wang & Wu, 2022).

Another anti-chlorine metabolism of *E. coli* biofilm was regulated by phosphorylcholine, an important precursor of membrane phospholipid (Geiger et al., 2013). HOCL could damage the cell membrane and induce cell lysis in order to penetrate and reach the intracellular constituents (Byun et al., 2021). The elevated level of phosphorylcholine upon chlorine indicated the activation of membrane recovery. Nikparvar, Subires, Capellas, Hernandez, and Bar (2019) also discovered that some pathogens can repair their membrane damage after environmental pressure and proposed a repair mechanism of the pathogen for their resistance against stress. Although in Wang and Wu (2022) study, phosphorylcholine was reported to decline after treating with electrolyzed water in *E. coli* O111, O26, O145, O103, and O157, it suggested that this bacterial self-recovery system might fail once exceed its tolerance or subject to the type of sanitizers. Moreover, phosphorylcholine could convert to betaine via choline formation, which is an essential osmoprotectant compound in *E. coli (*Zhao et al., 2019*)*. When the membrane integrity is damaged by chlorine, the increased production of betaine could help to maintain osmotic homeostasis (Zhao et al., 2022). Therefore, the observation of betaine increased in all strains further affirm the adaptive resistant response of *E. coli* biofilm to chlorine treatment.

4. Conclusion

In this research, the transfer rates of *E. coli* biofilms "big six" from food-contact surfaces to sponge cakes upon chlorine were studied as well as the effect of chlorine on metabolic changes of *E. coli* biofilms on SS and HDPE surfaces. Chlorine was effective to inhibit the adhesion of *E. coli* between surfaces and cakes, and a higher tolerance of *E. coli* biofilm on HDPE against chlorine was discovered. Overall, *E. coli* O45 displayed more metabolites affected on SS than on HDPE, whereas O157 the opposite. O145, O103, and O111 followed the same pattern of metabolic response on both surfaces upon chlorine. O121 and O26 had poor sensitivity to chlorine with a minimal degree of metabolic alterations on both surfaces. Further investigation found that the alterations in metabolic pathways were mostly associated with amino acid metabolism, energy metabolism, and anti-chlorine metabolism in response to oxidative and osmotic stressors. This research indicated that NMR-based metabolomics could be utilized to elucidate the antimicrobial mechanisms of chlorine against *E. coli* biofilms, which guides to prevent "big six" cross-contamination between food-contact surfaces and food.

CRediT authorship contribution statement

Zejia Lin: Conceptualization, Methodology, Investigation, Software, Visualization, Writing – original draft, Writing – review & editing. **Tong Chen:** Investigation, Methodology. **Lehao Zhou:** Investigation, Software. **Hongshun Yang:** Conceptualization, Funding acquisition, Project administration, Supervision, Writing – review & editing.

Declaration of Competing Interest

The authors declare that they have no known competing financial interests or personal relationships that could have appeared to influence the work reported in this paper.

Acknowledgements

This study was funded by Singapore Ministry of Education Academic Research Fund Tier 1 (R-160-000-A40-114), and an industry grant supported by Shanghai Congwu Industrial Co., Ltd (A-0004846-00-00).

Appendix A. Supplementary material

Supplementary data to this article can be found online at https://doi.org/10.1016/j.foodres.2022.111361.

References

Adhikari, A., Syamaladevi, R. M., Killinger, K., & Sablani, S. S. (2015). Ultraviolet-C light inactivation of *Escherichia coli* O157: H7 and *Listeria monocytogenes* on organic fruit surfaces. *International Journal of Food Microbiology, 210*, 136–142.

Araújo, E. A., Bernardes, P. C., Andrade, N. J., Fernandes, P. E., & Sá, J. P. N. (2009). Gibbs free energy of adhesion of *Bacillus cereus* isolated from dairy plants on different food processing surfaces evaluated by the hydrophobicity. *International Journal of Food Science Technology, 44*(12), 2519–2525.

Bakterij, A. J. M. T. (2014). An overview of the influence of stainless-steel surface properties on bacterial adhesion. *Materials and Technology, 48*, 609–617.

Bang, J., Hong, A., Kim, H., Beuchat, L. R., Rhee, M. S., Kim, Y., & Ryu, J.-H. (2014). Inactivation of *Escherichia coli* O157: H7 in biofilm on food-contact surfaces by sequential treatments of aqueous chlorine dioxide and drying. *International Journal of Food Microbiology, 191*, 129–134.

Byun, K.-H., Han, S. H., Yoon, J.-W., Park, S. H., & Ha, S.-D. (2021). Efficacy of chlorine-based disinfectants (sodium hypochlorite and chlorine dioxide) on *Salmonella Enteritidis* planktonic cells, biofilms on food contact surfaces and chicken skin. *Food Control, 123*, Article 107838.

Centers for Disease Control and Prevention (2021). Reports of Selected *E. coli* Outbreak Investigations. Retrieved from https://www.cdc.gov/ecoli/outbreaks.html.

Chen, L., Liu, Q., Zhao, X., Zhang, H., Pang, X., & Yang, H. (2022). Inactivation efficacies of lactic acid and mild heat treatments against *Escherichia coli* strains in organic broccoli sprouts. *Food Control, 133*, Article 108577.

Chen, L., Zhao, X., Wu, J. E., Liu, Q., Pang, X., & Yang, H. (2020). Metabolic characterisation of eight Escherichia coli strains including "Big Six" and acidic responses of selected strains revealed by NMR spectroscopy. *Food Microbiology, 88*, 103399.

Dhowlaghar, N., Bansal, M., Schilling, M. W., & Nannapaneni, R. (2018). Scanning electron microscopy of *Salmonella* biofilms on various food-contact surfaces in catfish mucus. *Food Microbiology, 74*, 143–150.

Di Ciccio, P., Vergara, A., Festino, A. R., Paludi, D., Zanardi, E., Ghidini, S., & Ianieri, A. (2015). Biofilm formation by *Staphylococcus aureus* on food contact surfaces: Relationship with temperature and cell surface hydrophobicity. *Food Control, 50*, 930–936.

Environmental Protection Agency (2020). *Section 180.940, Tolerance Exemptions for Active and Inert Ingredients for Use in Antimicrobial Formulations (Food-Contact Surface Sanitizing Solutions)*. Retrieved from https://www.govinfo.gov/app/details/CFR-2020-title40-vol26/CFR-2020-title40-vol26-sec180-940.

Food and Drug Administration (2022). Handling Flour Safely: What You Need to Know. Retrieved from https://www.fda.gov/food/buy-store-serve-safe-food/handling-flour-safely-what-you-need-know.

Geiger, O., López-Lara, I. M., & Sohlenkamp, C. (2013). Phosphatidylcholine biosynthesis and function in bacteria. *Biochimica et Biophysica Acta (BBA) – Molecular and Cell Biology of Lipids, 1831*(3), 503–513.

Guo, L., Sun, Y., Zhu, Y., Wang, B., Xu, L., Huang, M., … Sun, J. (2020). The antibacterial mechanism of ultrasound in combination with sodium hypochlorite in the control of *Escherichia coli*. *Food Research International, 129*, Article 108887.

Haiko, J., & Westerlund-Wikström, B. (2013). The Role of the Bacterial Flagellum in Adhesion and Virulence. *Biology, 2*(4), 1242–1267.

Han, D., Hung, Y.-C., Bratcher, C. L., Monu, E. A., Wang, Y., Wang, L., & Schottel, J. L. (2018). Formation of Sublethally Injured *Yersinia enterocolitica*, *Escherichia coli* O157: H7, and *Salmonella enterica* Serovar Enteritidis Cells after Neutral Electrolyzed Oxidizing Water Treatments. *Applied and Environmental Microbiology, 84*(17). e01066-01018.

He, Y., Zhao, X., Chen, L., Zhao, L., & Yang, H. (2021). Effect of electrolysed water generated by sodium chloride combined with sodium bicarbonate solution against *Listeria innocua* in broth and on shrimp. *Food Control, 127*, Article 108134.

Kim, C. Y., Ryu, G. J., Park, H. Y., & Ryu, K. (2017). Resistance of *Staphylococcus aureus* on food contact surfaces with different surface characteristics to chemical sanitizers. *Journal of Food Safety, 37*(4), Article e12354.

Kim, H., Moon, M. J., Kim, C. Y., & Ryu, K. (2019). Efficacy of chemical sanitizers against *Bacillus cereus* on food contact surfaces with scratch and biofilm. *Food Science and Biotechnology, 28*(2), 581–590.

Kim, W.-J., Kim, S.-H., & Kang, D.-H. (2020). Thermal and non-thermal treatment effects on *Staphylococcus aureus* biofilms formed at different temperatures and maturation periods. *Food Research International, 137*, Article 109432.

Koebmann, B. J., Westerhoff, H. V., Snoep, J. L., Nilsson, D., & Jensen, P. R. (2002). The glycolytic flux in *Escherichia coli* is controlled by the demand for ATP. *Journal of Bacteriology, 184*(14), 3909–3916.

Kwak, S. J., Jo, H. J., & Yoon, K. S. (2014). Effect of sodium hypochlorite (NaClO) sanitizer-induced stress on growth kinetics and morphological changes in *Escherichia coli* and *Bacillus cereus* spores. *Food Science and Biotechnology, 23*(3), 815–821.

Li, K., Chiu, Y.-C., Jiang, W., Jones, L., Etienne, X., & Shen, C. (2020). Comparing the Efficacy of Two Triple-Wash Procedures With Sodium Hypochlorite, a Lactic-Citric Acid Blend, and a Mix of Peroxyacetic Acid and Hydrogen Peroxide to Inactivate *Salmonella*, *Listeria monocytogenes* and Surrogate *Enterococcus faecium* on Cucumbers and Tomatoes. *Frontiers in Sustainable Food Systems, 4*.

Liu, Q., Chen, L., Laserna, A. K. C., He, Y., Feng, X., & Yang, H. (2020). Synergistic action of electrolyzed water and mild heat for enhanced microbial inactivation of *Escherichia coli* O157:H7 revealed by metabolomics analysis. *Food Control, 110*, Article 107026.

Liu, Y., Wu, L., Han, J., Dong, P., Luo, X., Zhang, Y., & Zhu, L. (2021). Inhibition of Biofilm Formation and Related Gene Expression of *Listeria monocytogenes* in Response to Four Natural Antimicrobial Compounds and Sodium Hypochlorite. *Frontiers in Microbiology, 11*(3523).

Lushchak, V. I. (2011). Adaptive response to oxidative stress: Bacteria, fungi, plants and animals. *Comparative Biochemistry and Physiology Part C: Toxicology & Pharmacology, 153*(2), 175–190.

Luu, P., Chhetri, V. S., Janes, M. E., King, J. M., & Adhikari, A. (2021). Efficacy of gaseous chlorine dioxide in reducing *Salmonella enterica*, *E. coli* O157: H7, and *Listeria monocytogenes* on strawberries and blueberries. *LWT, 141*, Article 110906.

Mahmud, I., Kousik, C., Hassell, R., Chowdhury, K., & Boroujerdi, A. F. (2015). NMR spectroscopy identifies metabolites translocated from powdery mildew resistant rootstocks to susceptible watermelon scions. *Journal of Agricultural Food Chemistry, 63*(36), 8083–8091.

McGlynn, W. G. (2004). *Food technology fact sheet: Guidelines for the use of chlorine bleach as a sanitizer in food processing operations*, Oklahoma USA.

Merino, L., Procura, F., Trejo, F. M., Bueno, D. J., & Golowczyc, M. A. (2019). Biofilm formation by *Salmonella* sp. in the poultry industry: Detection, control and eradication strategies. *Food Research International, 119*, 530–540.

Miranda, R. C., & Schaffner, D. W. (2016). Longer contact times increase cross-contamination of *Enterobacter aerogenes* from surfaces to food. *Applied and Environmental Microbiology, 82*(21), 6490–6496.

Munir, S., Li, Y., He, P., He, P., Ahmed, A., Wu, Y., & He, Y. (2020). Unraveling the metabolite signature of citrus showing defense response towards *Candidatus* Liberibacter asiaticus after application of endophyte *Bacillus subtilis* L1–21. *Microbiological Research, 234*, Article 126425.

Nikparvar, B., Subires, A., Capellas, M., Hernandez, M., & Bar, N. (2019). A Dynamic Model of Membrane Recovery Mechanisms in Bacteria following High Pressure Processing. *IFAC-PapersOnLine, 52*(1), 243–250.

Pagedar, A., Singh, J., & Batish, V. K. (2010). Surface hydrophobicity, nutritional contents affect *Staphylococcus aureus* biofilms and temperature influences its survival in preformed biofilms. *Journal of Basic Microbiology, 50*(S1), S98–S106.

Park, S.-H., & Kang, D.-H. (2017). Influence of surface properties of produce and food contact surfaces on the efficacy of chlorine dioxide gas for the inactivation of foodborne pathogens. *Food Control, 81*, 88–95.

Rahman, S., Ul Haq, F., Ali, A., Khan, M. N., Shah, S. M. Z., Adhikhari, A., … Musharraf, S. G. (2019). Combining untargeted and targeted metabolomics approaches for the standardization of polyherbal formulations through UPLC–MS/MS. *Metabolomics, 15*(9), 116.

Shen, C., Luo, Y., Nou, X., Bauchan, G., Zhou, B., Wang, Q., & Millner, P. (2012). Enhanced Inactivation of *Salmonella* and *Pseudomonas* Biofilms on Stainless Steel by Use of T-128, a Fresh-Produce Washing Aid, in Chlorinated Wash Solutions. *Applied and Environmental Microbiology, 78*(19), 6789–6798.

Sheng, L., Zhang, Z., Sun, G., & Wang, L. (2020). Light-driven antimicrobial activities of vitamin K3 against *Listeria monocytogenes*, *Escherichia coli* O157:H7 and *Salmonella Enteritidis*. *Food Control, 114*, Article 107235.

Small, D. A., Chang, W., Toghrol, F., & Bentley, W. E. (2007). Toxicogenomic analysis of sodium hypochlorite antimicrobial mechanisms in *Pseudomonas aeruginosa*. *Applied Microbiology and Biotechnology, 74*(1), 176–185.

Tan, J., & Karwe, M. V. (2021). Inactivation and removal of *Enterobacter aerogenes* biofilm in a model piping system using plasma-activated water (PAW). *Innovative Food Science & Emerging Technologies, 69*, Article 102664.

Tan, J., Yi, J., Yang, X., Lee, H., Nitin, N., & Karwe, M. (2022). Distribution of chlorine sanitizer in a flume tank: Numerical predictions and experimental validation. *LWT, 155*, Article 112888.

Tan, J., Zhou, B., Luo, Y., & Karwe, M. V. (2021). Numerical simulation and experimental validation of bacterial detachment using a spherical produce model in an industrial-scale flume washer. *Food Control, 130*, Article 108300.

Tkachenko, A., Nesterova, L., & Pshenichnov, M. (2001). The role of the natural polyamine putrescine in defense against oxidative stress in *Escherichia coli*. *Archives of Microbiology, 176*(1), 155–157.

Vong, W. C., Hua, X. Y., & Liu, S.-Q. (2018). Solid-state fermentation with *Rhizopus oligosporus* and *Yarrowia lipolytica* improved nutritional and flavour properties of okara. *LWT, 90*, 316–322.

von Hertwig, A. M., Prestes, F. S., & Nascimento, M. S. (2022). Biofilm formation and resistance to sanitizers by *Salmonella* spp. Isolated from the peanut supply chain. *Food Research International, 152*, Article 110882.

Wang, N., Jin, Y., He, G., & Yuan, L. (2021a). Development of multi-species biofilm formed by thermophilic bacteria on stainless steel immerged in skimmed milk. *Food Research International, 150*, Article 110754.

Wang, W., Sang, Y., Liu, J., Liang, X., Guo, S., Liu, L., … Wang, L. (2021b). Identification of novel monoclonal antibodies targeting the outer membrane protein C and lipopolysaccharides for *Escherichia coli* O157:H7 detection. *Journal of Applied Microbiology, 130*(4), 1245–1258.

Wang, Y., Wu, J. E., & Yang, H. (2022). Comparison of the metabolic responses of eight *Escherichia coli* strains including the "big six" in pea sprouts to low concentration electrolysed water by NMR spectroscopy. *Food Control, 131*, 108458.

Weerarathne, P., Payne, J., Saha, J., Kountoupis, T., Jadeja, R., & Jaroni, D. (2021). Evaluating the efficacy of sodium acid sulfate to reduce *Escherichia coli* O157:H7 and its biofilms on food-contact surfaces. *LWT, 139*, Article 110501.

Winaya, A., Maftuchah, & Zainudin, A. (2020). The identification of osmoprotectant compounds from Jatropha curcas Linn. plant for natural drought stress tolerance. *Energy Reports, 6*, 626–630.

Wu, J., Zhao, L., Lai, S., & Yang, H. (2021). NMR-based metabolomic investigation of antimicrobial mechanism of electrolysed water combined with moderate heat treatment against *Listeria monocytogenes* on salmon. *Food Control, 125*, Article 107974.

Xue, Z., Sendamangalam, V. R., Gruden, C. L., & Seo, Y. (2012). Multiple Roles of Extracellular Polymeric Substances on Resistance of Biofilm and Detached Clusters. *Environmental Science & Technology, 46*(24), 13212–13219.

Yang, L., Mih, N., Anand, A., Park, J. H., Tan, J., Yurkovich, J. T., … Palsson, B. O. (2019). Cellular responses to reactive oxygen species are predicted from molecular mechanisms. *Proceedings of the National Academy of Sciences, 116*(28), 14368.

Ying, W., Yang, F., Bick, A., Oron, G., & Herzberg, M. (2010). Extracellular Polymeric Substances (EPS) in a Hybrid Growth Membrane Bioreactor (HG-MBR): Viscoelastic and Adherence Characteristics. *Environmental Science & Technology, 44*(22), 8636–8643.

Zhang, W., Chen, X., Sun, W., Nie, T., Quanquin, N., & Sun, Y. (2020). *Escherichia coli* Increases its ATP Concentration in Weakly Acidic Environments Principally through the Glycolytic Pathway. *Genes, 11*(9).

Zhao, L., Li, S., & Yang, H. (2021). Recent advances on research of electrolyzed water and its applications. *Current Opinion in Food Science, 41*, 180–188.

Zhao, L., Poh, C. N., Wu, J., Zhao, X., He, Y., & Yang, H. (2022). Effects of electrolysed water combined with ultrasound on inactivation kinetics and metabolite profiles of *Escherichia coli* biofilms on food contact surface. *Innovative Food Science & Emerging Technologies, 76*, Article 102917.

Zhao, L., Zhang, Y., & Yang, H. (2017). Efficacy of low concentration neutralised electrolysed water and ultrasound combination for inactivating *Escherichia coli* ATCC 25922, *Pichia pastoris* GS115 and *Aureobasidium pullulans* 2012 on stainless steel coupons. *Food Control, 73*, 889–899.

Zhao, L., Zhao, M. Y., Phey, C. P., & Yang, H. (2019). Efficacy of low concentration acidic electrolysed water and levulinic acid combination on fresh organic lettuce (*Lactuca sativa* Var. *Crispa* L.) and its antimicrobial mechanism. *Food Control, 101*, 241–250.

Zhao, X., Chen, L., Wu, J. E., He, Y., & Yang, H. S. (2020). Elucidating antimicrobial mechanism of nisin and grape seed extract against *Listeria monocytogenes* in broth and on shrimp through NMR-based metabolomics approach. *International Journal of Food Microbiology, 319*.